Supporting Information

Understanding the Desulphurization Process in an Ionic Porous Aromatic Framework

Yuyang Tian, Jian Song, Youliang Zhu, Huanyu Zhao, Faheem Muhammad, Tingting Ma, Mo Chen, and Guangshan Zhu *

Table of Contents

Section S1	**Materials and Methods**	**Page 2**
Section S2	**Synthetic Procedure**	**Page 4**
Section S3	**Characterizations**	**Page 9**
Section S4	**DBT adsorption models for iPAF-1**	**Page 14**
Section S5	**Computational Simulation**	**Page 16**
Section S6	**References**	**Page 20**

Section S1. Materials and Methods:

Materials:

All chemicals were used as received without further purification. 2,2'-bipyridyl, 1,5-cyclooctadiene (cod) and bis(1,5-cyclooctadiene)nickel(0) ([Ni(cod)$_2$]) were obtained from Aldrich (Beijing) Development Co., Ltd. Dehydrated Dimethylformamide (DMF), trityl chloride, o-toluidine, Isoamyl nitrite, N-bromosuccinimide and benzoyl peroxide were obtained from TCI (Shanghai) Development Co., Ltd.

General instrumentation and methods:

^{1}H NMR spectra were recorded on Varian Unity Inova 500 MHz NMR spectrometer. TGA was measured on the Netzch Sta 449c thermal analyzer at the 10°C min^{-1} heating rate in air atmosphere. FT-IR measurements were performed on the Nicolet Impact 410 Fourier transforms infrared spectrometer. N_2-adsorption isotherms and pore size distribution were obtained on the Micromeritics ASAP 2010M analyzer. SEM and EDS were implemented on the JEOS JSM 6700. XRD patterns were carried out on the Riguku D/MAX 2550 diffractometer using CuKα radiation, 40 kV, 200 mA. XPS was implemented on the AXIS ULTRA. The Elemental analysis (for C, H, and N) was measured using a Perkin Elmer 2400 Series II CHNS/O Analyzer. S contents were determined by Gas Chromatography equipped with Flame Ionization Detector (GC-FID) (Agilent 7890A; DB-1701, 30 m x 0.32 mm x 0.25 μm; FID: Agilent).

Desulphurization experiments:

The desulphurization performance of iPAF-1 was tested by batch experiments. The model gasoline oil was prepared by dissolving dibenzothiophene (DBT) with various concentrations in n-octane. In a typical experiment, 10 mg of iPAF-1 was mixed with the gasoline (10 mL) in a glass bottle and stirred for a certain time at room temperature. Then, the adsorbents were centrifuged to be separated from the oil. The concentrations of sulphur in the gasoline before and after desulphurization were determined by GC.

The adsorbed amount (q_e) of the sulphur compounds was calculated by the following equation 1:

$$q_e = \frac{(C_0 - C_e)\,V}{m} \qquad \textit{(eq. 1)}$$

Whereas C_0 and C_e (mg L^{-1}) are the initial sulphur concentration and the equilibrium Sulphur concentration, respectively, V (L) is the volume of the oil, and m (g) is the mass of adsorbent.

The adsorption isotherms can be obtained by plotting the amount of sulphur compounds adsorbed at equilibrium (q_e) against the equilibrium concentration of sulphur in the model oil (C_e), and the results were fitted by the Langmuir adsorption model, which can be described as equation 2:

$$\frac{C_e}{q_e} = \frac{C_e}{q_m} + \frac{1}{q_m K_L} \qquad \textit{(eq. 2)}$$

Where q_m show the amount of sulphur compounds adsorbed corresponding to the complete monolayer coverage (mg DBT g^{-1}), and K_L is the Langmuir constant (L mg^{-1}). Therefore, the maximum complete adsorption amount q_m, can be obtained from the reciprocal of the slope of the plot of C_e/q_e against C_e.

Furthermore, the kinetics studies were based on the pseudo-second-order model as equation 3:

$$\frac{t}{q_t} = \frac{1}{k_2 q_e^2} + \frac{t}{q_e} \qquad \textit{(eq. 3)}$$

Where t (h) is the adsorption time, q_t is the amount of sulphur compounds adsorbed at time t, (mg DBT g^{-1}), q_e is the amount of sulphur compounds saturated adsorbed (mg g^{-1}) and k_2 is the pseudo-second-order-rate constant (g [mg h]$^{-1}$). The rate constant k_2 can be obtained from the slope and the intercept of the plot of t/q_t versus t.

The recycle use of iPAF-1 was achieved by washing the adsorbent with n-octane and ethanol to remove the adsorbed DBT and then filtrated and dried at 100 °C overnight. The stability of the desulphurization performance of the regenerated adsorbent was tested by repeating the desulphurization test.

Dibenzothiophene micro-breakthrough testing was performed using a micro-breakthrough apparatus. Samples of ~1 g were packed between two cotton wool plugs in a glass tube with an internal diameter of 2 cm. Dibenzothiophene at a sulphur concentration of 100 ppm was passed through the sample at a flow rate of 3 ml min^{-1} and the challenge sulphur output concentration was monitored using the Gas Chromatography.

Section S2. Synthetic Procedure:

Preparation of tetrakis(4-bromophenyl)methane monomers, Compounds 1-3, were synthesized following a modified literature procedure.[S1]

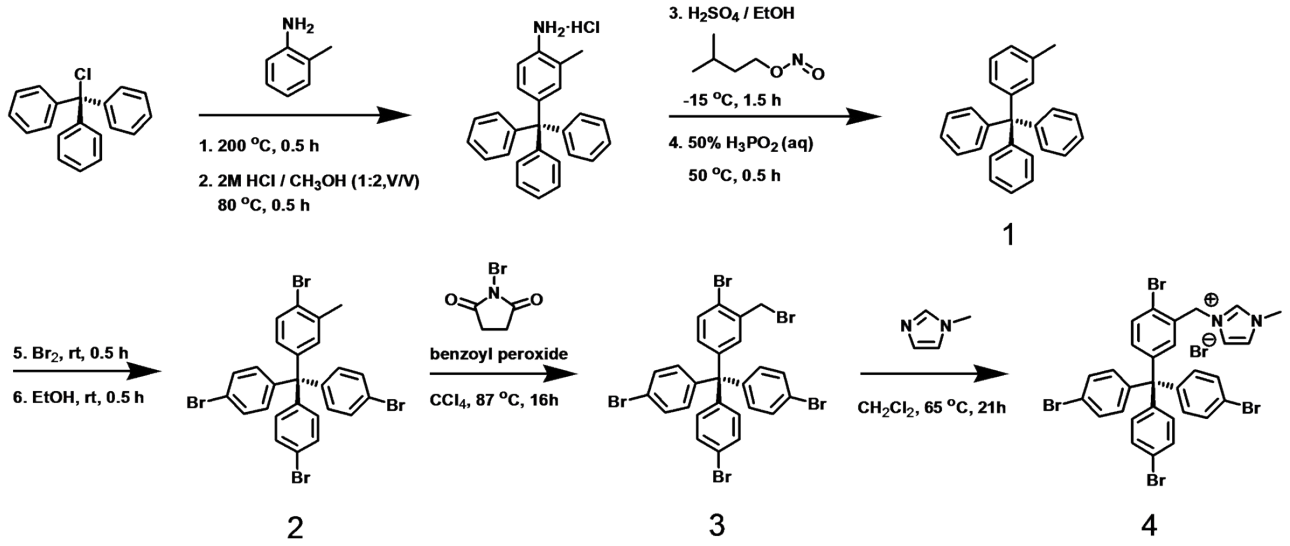

Figure S1. Schematic route to the synthesis of iTBPM.

Synthesis of (3-Methylphenyl)triphenylmethane (Compound 1).

Trityl chloride (9.2 g, 32.9 mmol) and *o*-toluidine (9.4 mL, 88.8 mmol) were added into a 250 mL round-bottom flask equipped with a water-cooled reflux condenser and a magnetic stirring bar. This mixture was stirred under reflux for 0.5 h. The resulting purple slurry reaction mixture was allowed to cool to room temperature when solidified. This solid was grounded with a spatula and the resulting powder was combined with a mixture of 2M HCl and methanol (25 mL /60 mL). The reflux condenser was reattached and the mixture was then heated at 80 °C for 0.5 h. After cooling to room temperature, the reaction mixture was filtered and washed with DI H_2O (125 mL) to afford a light purple solid, which was briefly air-dried on a Büchner funnel.

Into a 250 mL round-bottom flask equipped with a magnetic stirring bar were combined the crude 3-methyl-4-aminotetraphenylmethane salt, ethanol (65 mL), and concentrated H_2SO_4 (10 mL, 96 wt %). The resulting mixture was then cooled down to -15 °C. Isoamyl nitrite (7.5 mL, 55.8 mmol) was then added slowly over a 10 min period and the resulting mixture was stirred at -15 °C for 1 h. Aqueous hypophosphoric acid (15 mL, 50 %) was then added to the reaction mixture at -15 °C and the resulting mixture was warmed up to room temperature before being stirred at 50 °C for 2 h. The resultant precipitate was collected by suction filtration and washed with DI H_2O (100 mL) and ethanol (100 mL). The tan brown crude product (8.6 g, 25.6 mmol, 78%) was collected without any further purification. ^1H

NMR (499.8 MHz, $CDCl_3$): δ 2.26 (3H, C*H*$_3$), 7.00 (1H, Ar-*H*), 7.01 (1H, Ar-*H*), 7.03 (1H, Ar-*H*), 7.14 (1H, Ar-*H*), 7.18 to 7.25 (15H, trityl Ar-*H*).

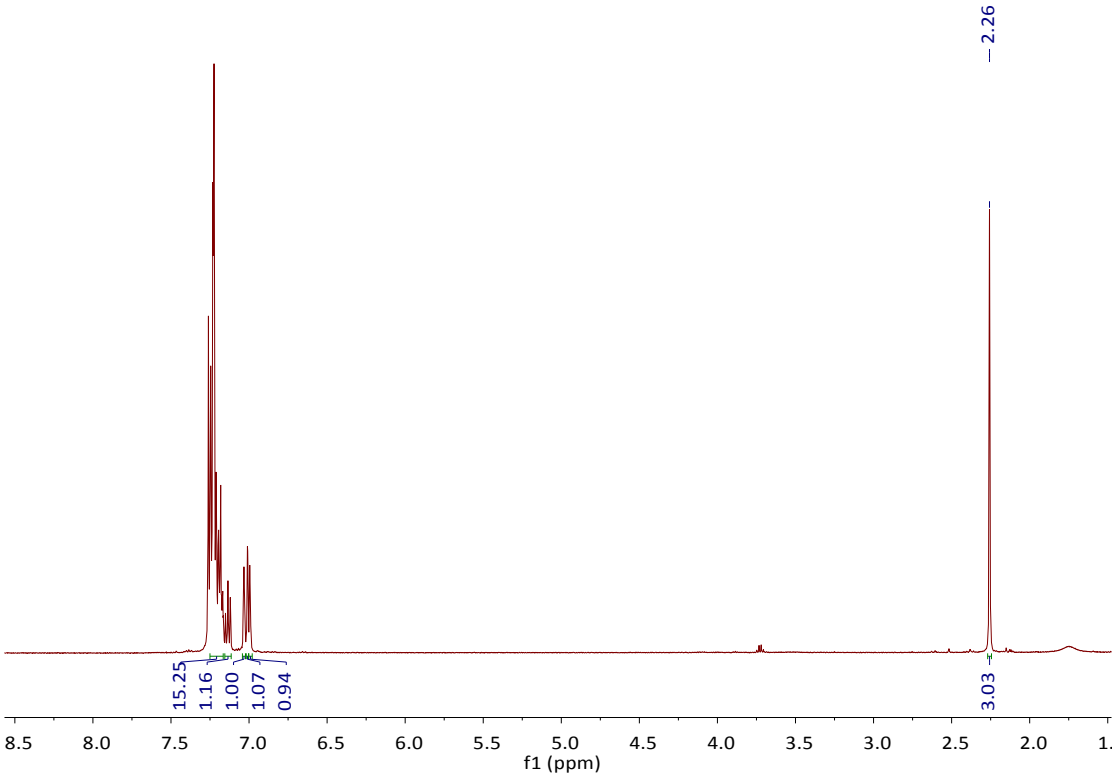

Figure S2. ^{1}H NMR spectrum of (3-Methylphenyl)triphenylmethane (Compound 1).

Synthesis of (4-Bromo-3-methylphenyl)tris(4-bromophenyl)methane (Compound 2).

A 150 mL 2-neck round-bottom flask equipped with a magnetic stir bar was charged with compound **1** (crude mass of 3.0 g, 8.96 mmol). One of the two necks was fitted with a rubber septum and the other one was then fitted with a side arm adapter that is connected to the fumehood. Neat bromine (3.5 mL, 67.3 mmol) was added dropwise through the septum via a syringe within 5 minutes before the resulting solution was allowed to stir at room temperature for 0.5 h. Ethanol (60 mL) was then added to the reaction mixture and the reaction was allowed to stir for an additional 0.5 h. The resultant precipitate was collected by suction filtration and washed with 150 mL of ethanol. The collected crude product was then purified by column chromatography to afford **2** (4.9 g, 7.6 mmol, 85%) as a white solid. ^{1}H NMR (499.8 MHz, $CDCl_3$): δ 2.30 (3H, C*H*$_3$), 6.80 (1H, Ar-*H*), 6.98 (1H, Ar-*H*), 7.02 (6H, trityl Ar-*H*), 7.38 (6H, trityl Ar-*H*), 7.41 (1H, Ar-*H*).

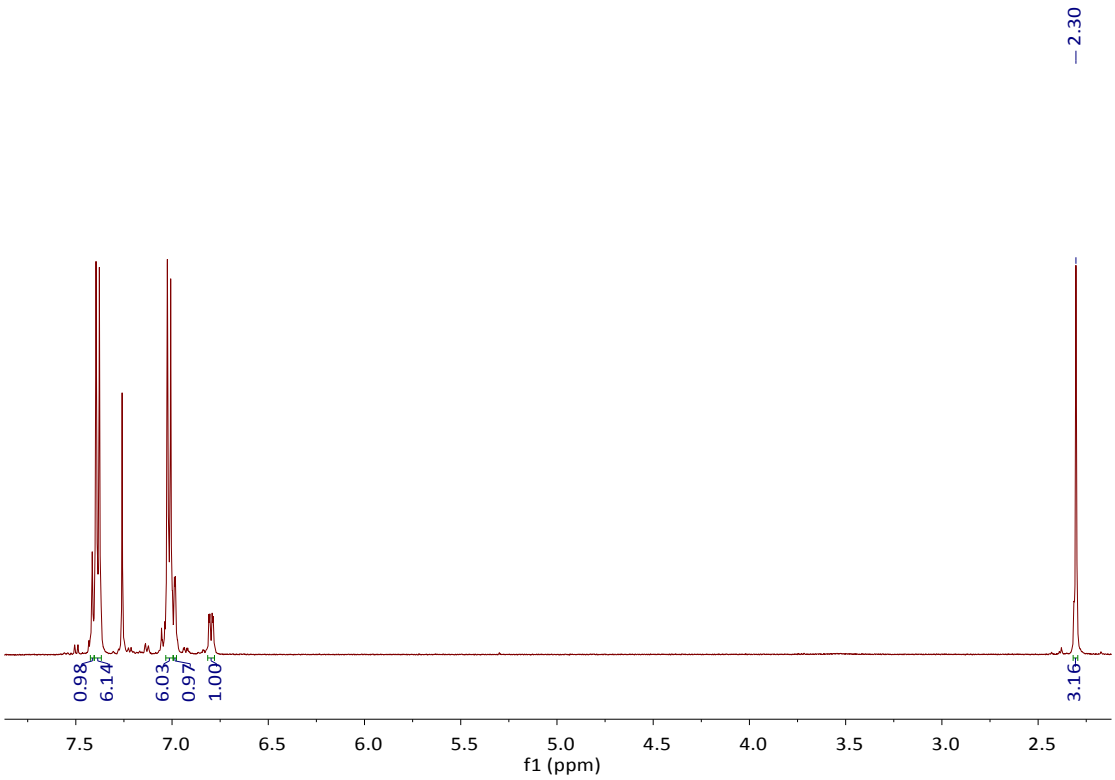

Figure S3. ^{1}H NMR spectrum of (4-Bromo-3-methylphenyl)tris(4-bromophenyl)methane (Compound 2).

Synthesis of (4-Bromo-3-(bromomethyl)phenyl)tris(4-bromophenyl)methane (Compound 3).

Compound **2** (1.0 g, 1.53 mmol) was dissolved with anhydrous CCl_4 (40 mL) in a 100 mL round bottom flask equipped with a magnetic stirring bar. This mixture was degassed with a stream of nitrogen for 10 minutes. N-bromosuccinimide (0.356 g, 1.99 mmol) and benzoyl peroxide (0.010 g, 0.04 mmol) were then added under N_2, and the reaction mixture was refluxed under nitrogen overnight. The reaction mixture was cooled to room temperature and filtered. The filtrate was concentrated to dry under reduced pressure to give pale yellow oil, which was triturated with 25 mL of ethanol to give an off-white powder. The collected crude product was then purified by column chromatography to afford **3** (2.6 g, 4.0 mmol, 45%) as an off-white powder. ^{1}H NMR (499.8 MHz, $CDCl_3$): δ 4.49 (2H, C*H*$_2$Br), 6.93 (1H, Ar-*H*), 7.01 (6H, trityl Ar-*H*), 7.23 (1H, Ar-*H*), 7.41 (6H, trityl Ar-*H*), 7.47 (1H, Ar-*H*).

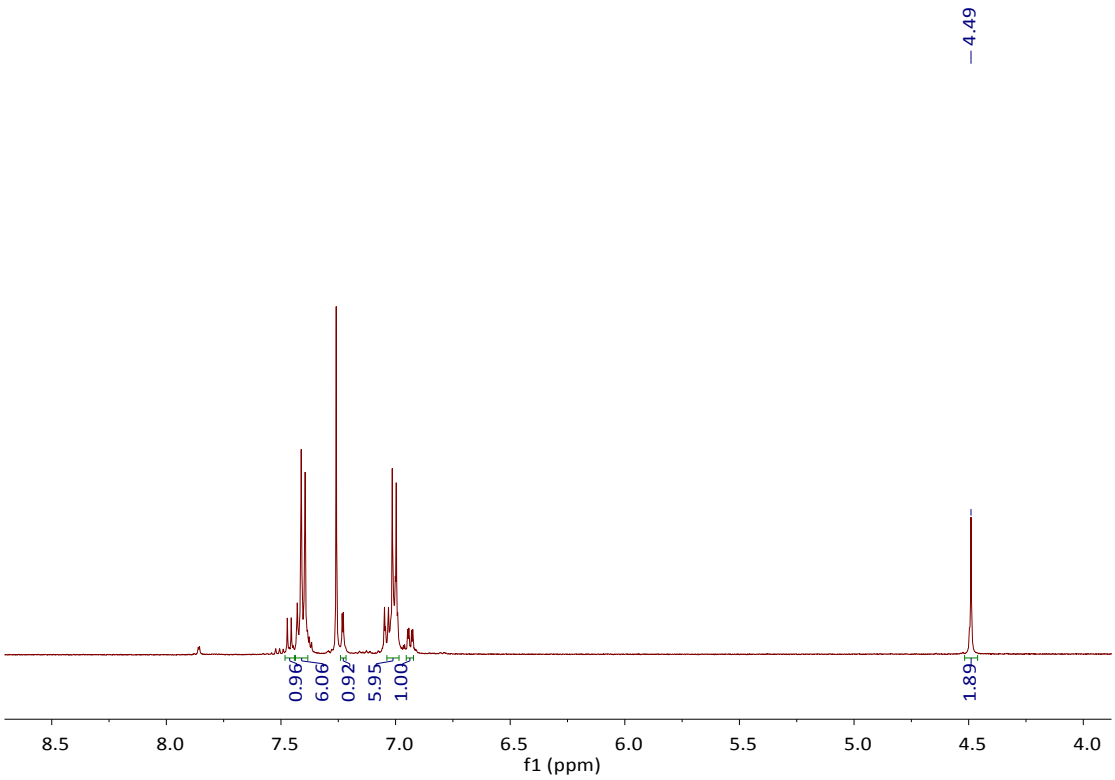

Figure S4. ^{1}H NMR spectrum of (4-Bromo-3-(bromomethyl)phenyl)tris(4-bromophenyl)methane (Compound 3).

Synthesis of (4-Bromo-3-(3-methylimidazolemethyl)phenyl)tris(4-bromophenyl)methane (iTBPM).

Compound **3** (1.0 g, 1.53 mmol) and N-methylimidazole (0.356 g, 1.99 mmol) was dissolved with 40 mL of CH_2Cl_2 in a 100 mL round bottom flask equipped with a magnetic stir bar and a rubber septum. A water-cooled reflux condenser was attached to the flask, and the reaction mixture was refluxed overnight. The reaction mixture was cooled to room temperature and filtered. The white powder was washed with ethyl acetate, which was collected by filtration and dried under vacuum (1.10 g, 1.5 mmol, 98%). ^{1}H NMR (499.8 MHz, $CDCl_3$, Fig. S5): δ 3.87 (3H, C*H*$_3$), 5.45 (2H, C*H*$_2$Br), 6.94 (1H, Ar-*H*), 7.06 (6H, trityl Ar-*H*), 7.09 (1H, Ar-*H*), 7.52 (6H, trityl Ar-*H*), 7.60 (1H, Ar-H), 7.70 (2H, Imidazol-*H*), 9.08 (1H, Imidazol-*H*).

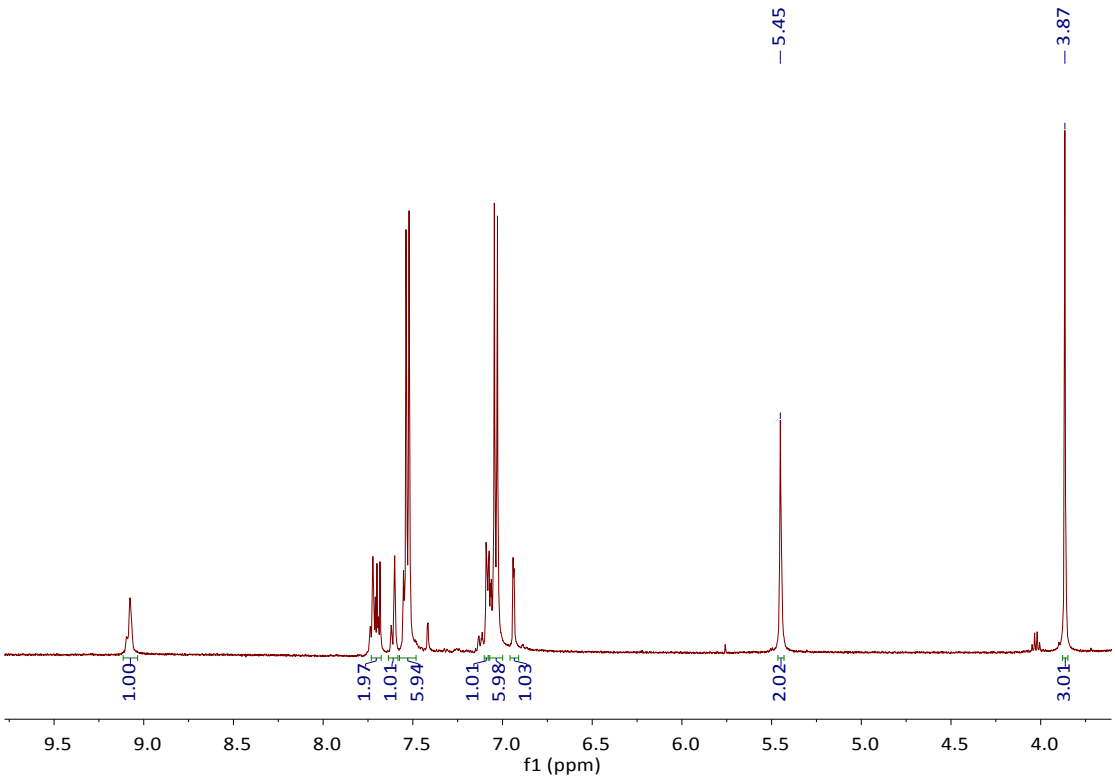

Figure S5. ^{1}H NMR spectrum of (4-Bromo-3-(3-methylimidazolemethyl)phenyl)tris(4-bromophenyl)methane (iTBPM).

Synthesis of iPAF-1

Regards to the synthesis of 3imidazolium modified PAF called iPAF-1, the 1,5-cyclooctadiene (cod, 1.05 mL, 8.32 mmol) was added to a clear solution of bis(1,5-cyclooctadiene)nickel(0) ([Ni(cod)$_2$], 2.25 g, 8.18 mmol) and 2,2'-bipyridyl (1.28 g, 8.18 mmol) in anhydrous DMF (120 mL), then reaction mixture was heated at 80°C for 1 h. After that, to the resulting purple solution, (4-Bromo-3-(3-methylimidazolemethyl)phenyl)tris(4-bromophenyl)methane (iTBPM, 1.27 g, 1.57 mmol) was added and the reaction mixture were stirred overnight at the same temperature to give a deep purple suspension. After cooling to room temperature, concentrated HCl was added to the mixture. After filtration, the residue was washed with DI H_2O and THF respectively, to afford a light yellow powder that was then Soxhlet extracted with THF for 48h (576 mg, 81% yields).

Section S3. Characterizations:

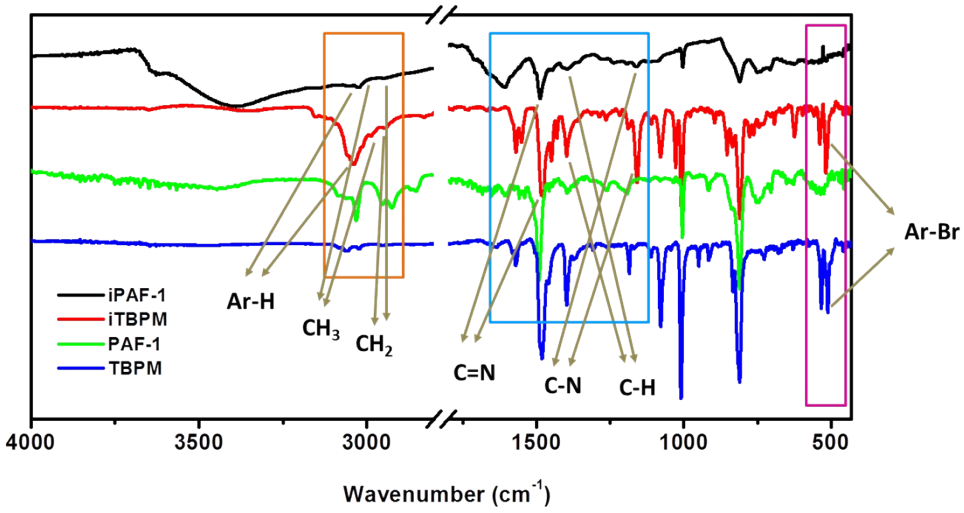

Figure S6. FT-IR spectra of iTBPM, iPAF-1, TBPM and PAF-1.

Table S1. Peak assignment for the FT-IR spectra of iTBPM and iPAF-1.

Peak (cm^{-1})	Assignment and notes
3410	O-H stretching from water in the iPAF-1 sample.
3037	Aromatic C—H stretching from phenyl rings.
2980, 2940	Aliphatic C—H stretching from CH_3 and CH_2.
1607, 1488	Aromatic ring C=C stretching and imidazolium ring C=N stretching.
1393	Imidazolium ring C-H stretching.
1160	Imidazolium ring C-N stretching.
537, 517	C—Br stretching from bromophenyl in iTBPM. The intense characteristics bands are completely disappeared in iPAF-1, indicating that the Ph-Br groups of the monomer iTBPM almost completely cross-coupled in PAF-1 derivative network.

Table S2. C, H and N elemental analysis of iTBPM and iPAF-1.

Sample		% C	% H	% N
iTBPM	Calcd ($C_{30}H_{23}N_2Br_5$)	44.42	2.84	3.45
	Found	44.993	2.25	3.682
iPAF-1	Calcd $(C_{30}H_{23}N_2Cl)_n$	80.63	5.15	6.27
	Found	74.828	5.107	6.074

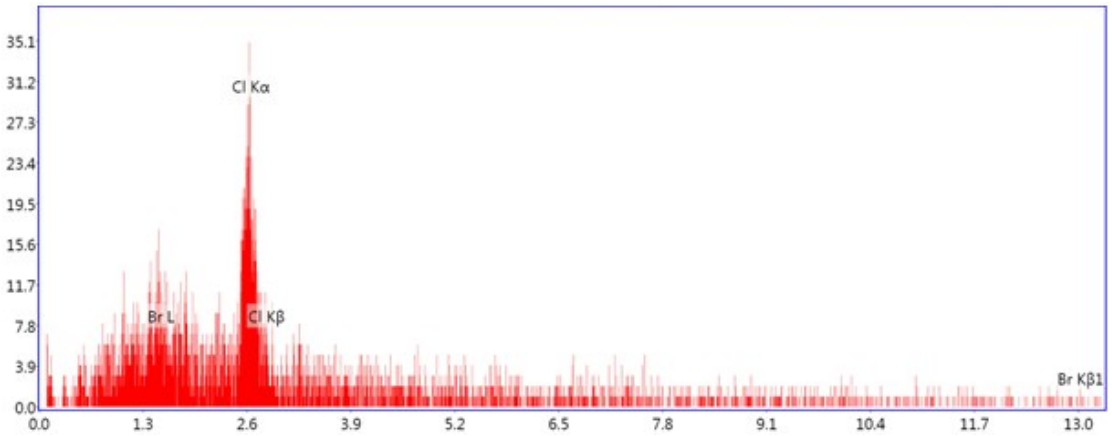

Element	Atom %
Br L	5.42
Cl K	94.58

Figure S7. EDS elemental analyses of iPAF-1 with halide ions.

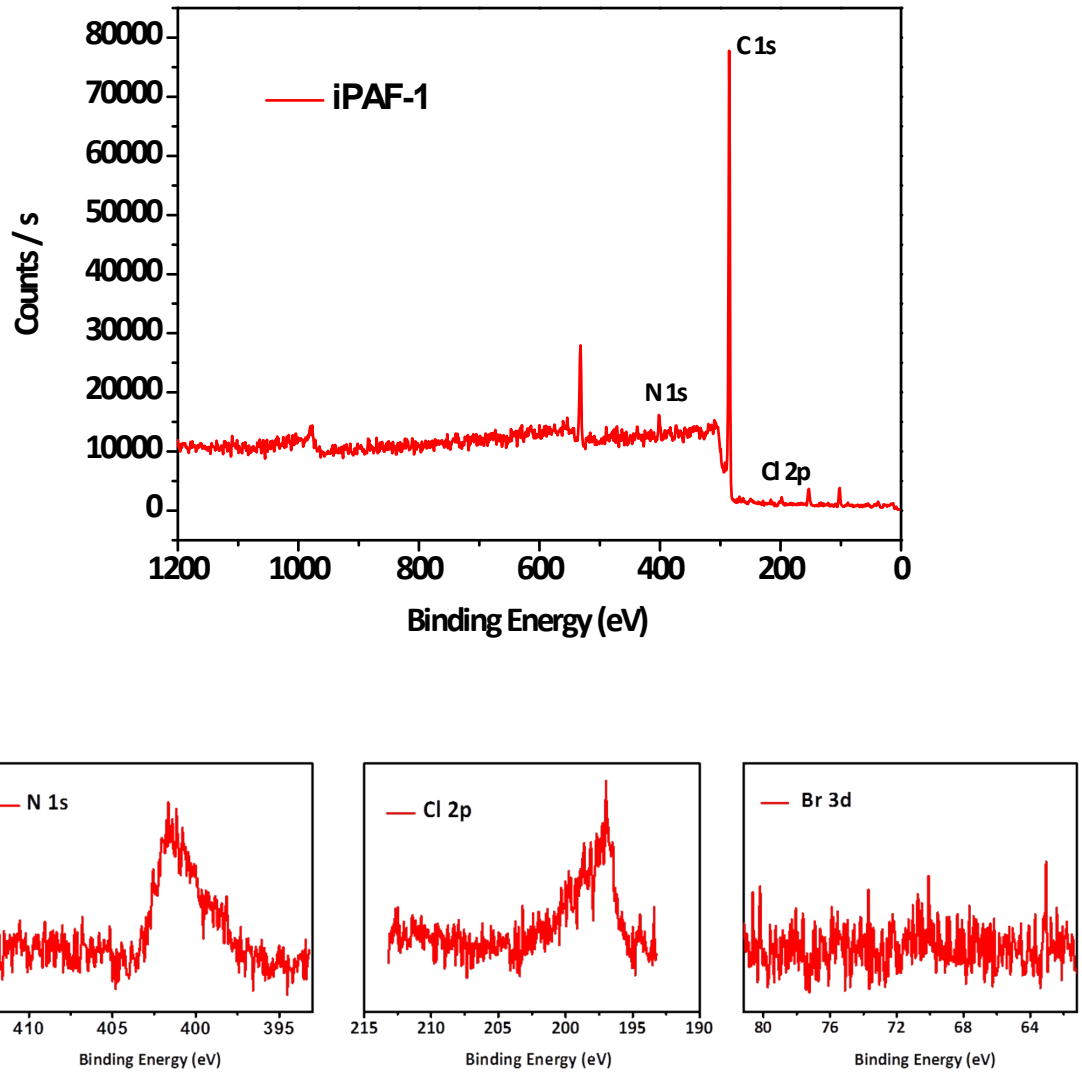

Figure S8. XPS spectra of iPAF-1 and enlarged views of XPS spectra of N 1s, Cl 2p, Br 3d in iPAF-1.

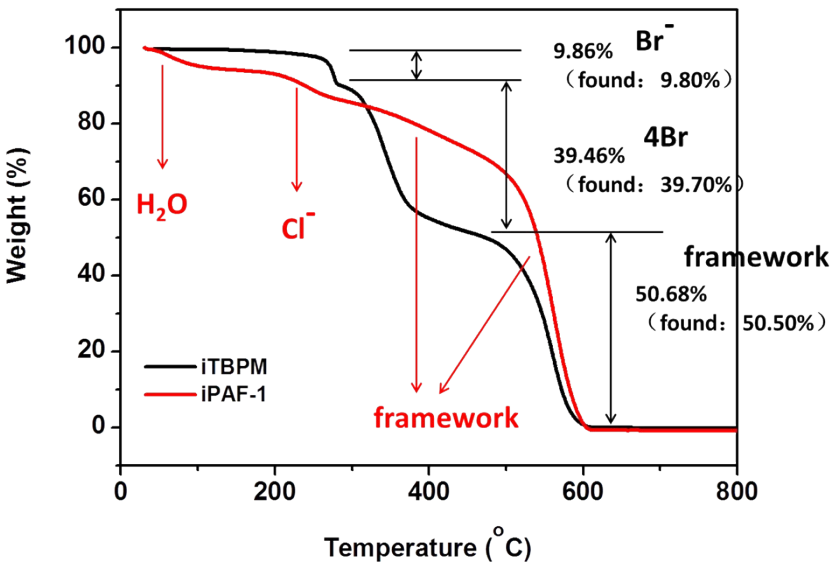

Figure S9. TG curves of of iTBPM and iPAF-1.

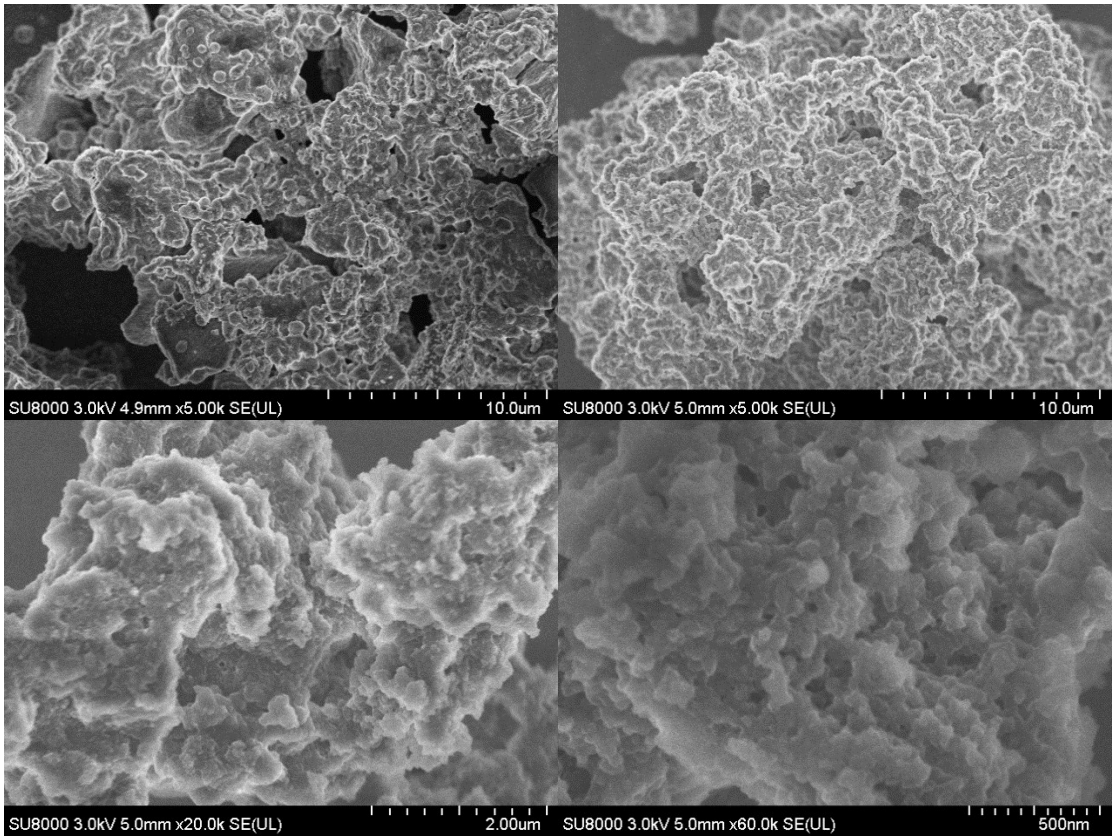

Figure S10. SEM images of iPAF-1.

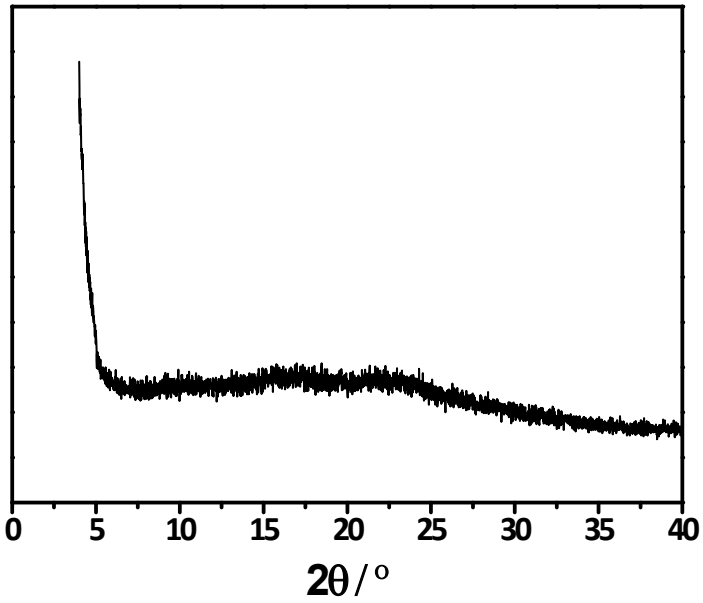

Figure S11. Powder X-ray diffraction pattern of iPAF-1.

Section S4. DBT adsorption model for iPAF-1:

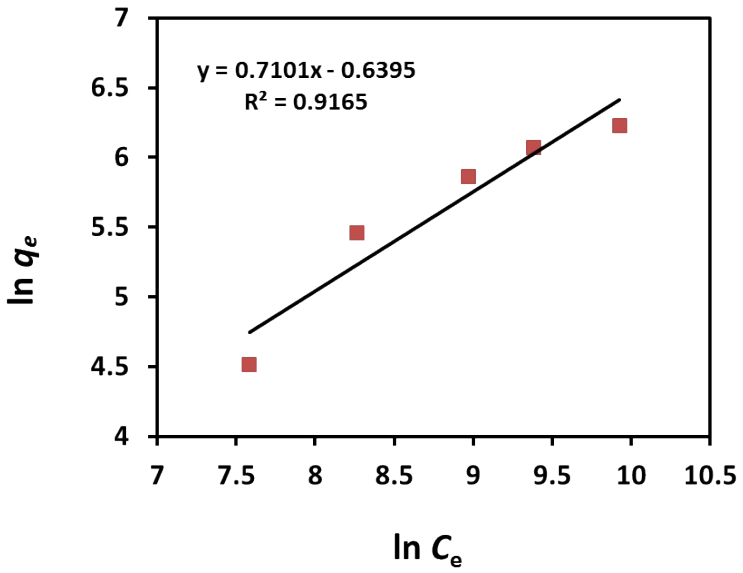

Figure S12. Freundlich model fitting of DBT adsorption for iPAF-1.

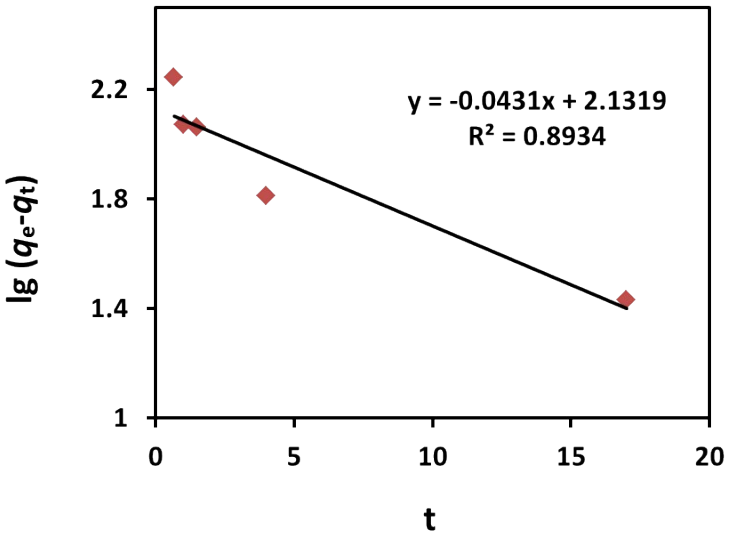

Figure S13. The plots of pseudo-first-order kinetic model of DBT adsorption for iPAF-1.

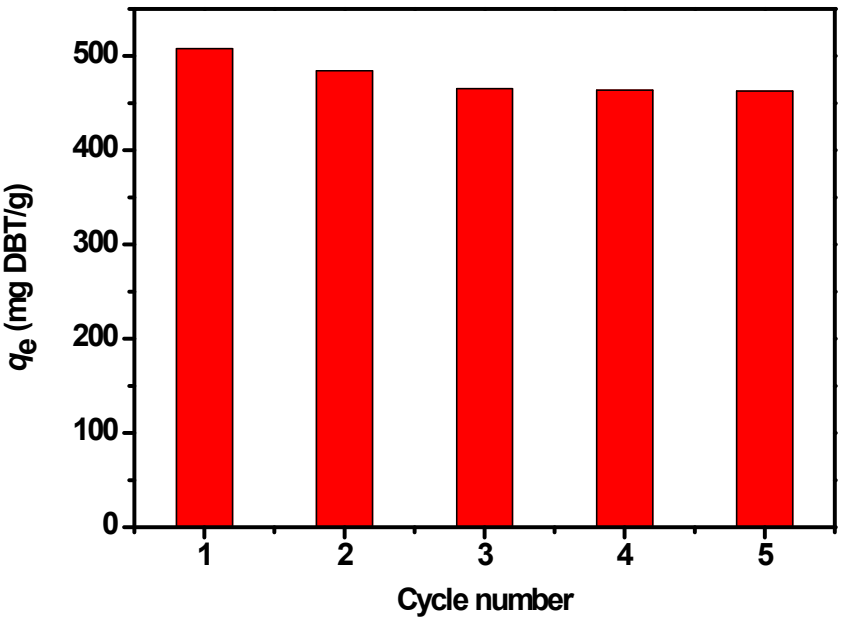

Figure S14. The recycle adsorption performance of DBT (20000 mg DBT·L^{-1}) for iPAF-1.

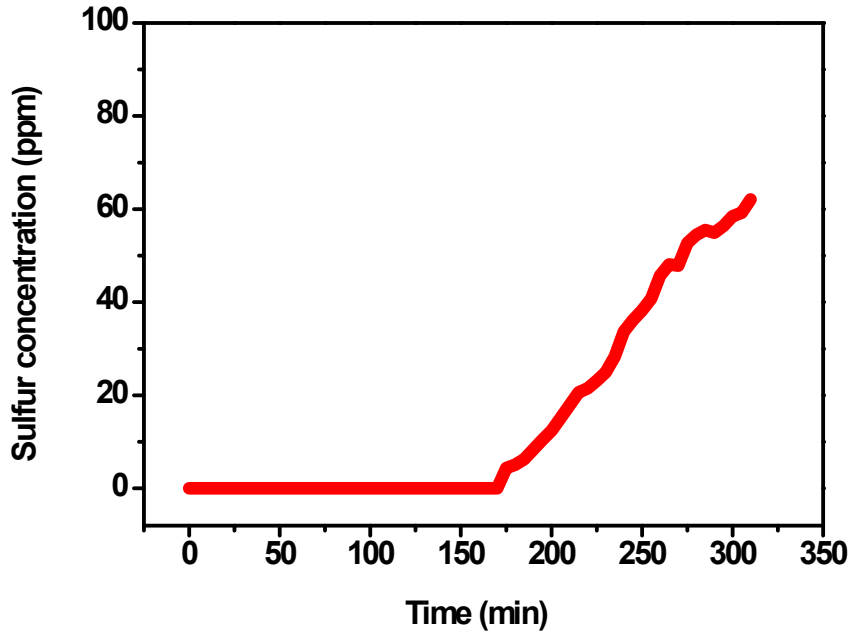

Figure S15. Breakthrough-curve of continuous DBT removal from model gasoline oil at a sulphur concentration of 100 ppm using iPAF-1.

Section S5. Computational Simulation:

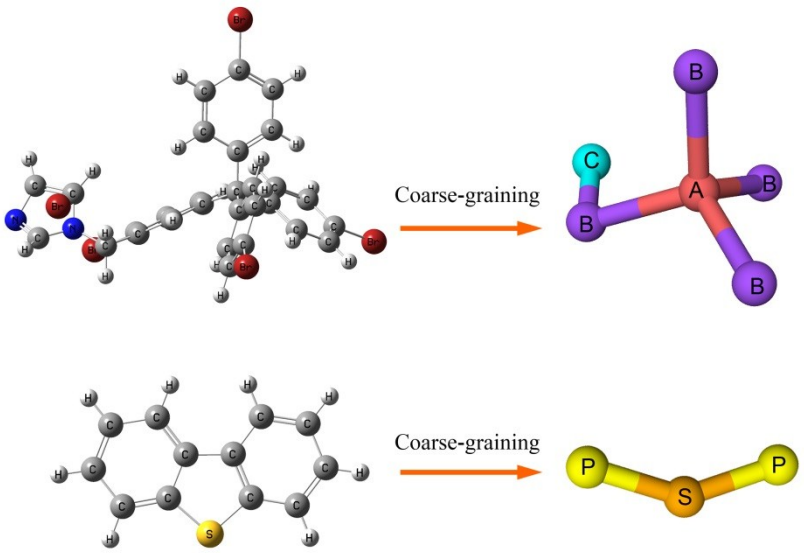

Figure S16. The CG models for iTBPM and DBT.

S5.1 Considering the large spatial and temporal scales of desulphurization process, we employ coarse-graining (CG) simulations to give an insight to the desulphurization phenomenon. Before doing that, we use a polymerization model to simulate the fabrication of the porous aromatic framework and study its structure. In particular, we build up the coarse-grained models of imidazolium precursor iTBPM and DBT. The CG models for iTBPM and DBT are shown in Fig. S16. In the CG model of iTBPM, the particle A represents the quaternary carbon center linked to four benzene groups. The particle B represents the reactable brominated benzene group and has the position of benzene group center. The particle C represents imidazole group and has the position of it center. In the CG model of DBT, particle P and S represents benzene group and thiophene group and have the position of their centers, respectively.

We employ Lennard-Jones (LJ) potential to describe the interactions between particles.

$$V_{\mathrm{LJ}}(r) = 4\varepsilon\left[\left(\frac{\sigma}{r}\right)^{12} - \left(\frac{\sigma}{r}\right)^{6}\right] \qquad \textit{(eq. 4)}$$

The ε = 0.2 kJ/mol is used for all type pairs except for ε_{CS}. The ε_{CS} is the binding energy between imidazole and thiophene, which is obtained by quantum chemistry calculation. The σ = 0.45 nm for all type pairs. We use harmonic potential to describe both bond stretching and angle bending interactions. The parameters for these two bonded interactions are listed.

$$V_{\text{bond}}(r) = \frac{1}{2} K_{\text{bond}} (r - r_0)^2 \qquad \textit{(eq. 5)}$$

Table S3. Parameters of bond stretching interactions

bonds	r_0 [nm]	K_{bond} [kJ mol^{-1} nm^{-2}]
A-B	0.30	1250
B-B	0.45	1250
B-C	0.40	1250
S-P	0.24	1250

$$V_{\text{angle}}(r) = \frac{1}{2} K_{\text{angle}} (\theta - \theta_0)^2 \qquad \textit{(eq. 6)}$$

Table S4. Parameters of angle bending interactions

angles	Θ_0 [degree]	K_{angle} [kJ mol^{-1}]
B-A-B	109.466	500.0
A-B-C	90.0	50.0
A-B-B	180.0	200.0
B-B-C	90.0	50.0
P-S-P	144	500.0

The particles are integrated forward in time according to the Langevin equations of motion with a time step dt =0.002. The drag coefficient is in default 1.0. The solvent is implied with the Langevin dynamics. Thereby, the LJ parameter ε = 0.2 kJ/mol represents a dissolved energy. The small value indicates a good solvent environment. The fundamental units in simulation of mass, length, and energy are [amu], [nm], and [kJ/mol], respectively. Thereby, the real unit of time is picosecond. We construct a box of the size of 15 nm*15 nm*30 nm and initially place 7000 iTBPM

molecules randomly in the box (Fig. S17). The CG simulations are all performed on GPU by the MD software GALAMOST.[S2-S4]

The intermolecular particle B could react with each other in the polymerization model. The reaction simulation is performed every 50 timesteps with a probability of P_r=0.0001. In a reaction event, a B-B bond, two A-B-B angles, and a B-B-C angle will be newly generated and their interactions are imposed on relevant particles since then (Fig. S18). We perform the simulation of B and B reaction for $5*10^7$ time steps. The total simulation time is 10^5, which is long enough for the full reaction. About 90% B particles are finally reacted according to our statistics (Fig. S19).

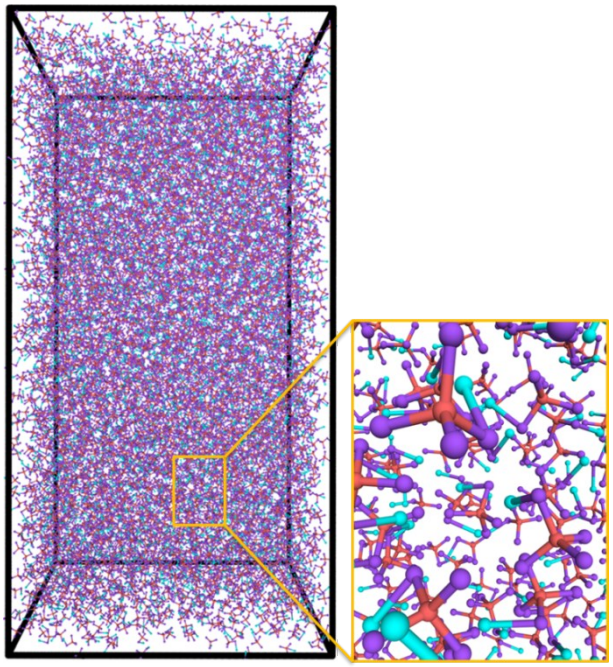

Figure S17. The 7000 iTBPM molecules in the box.

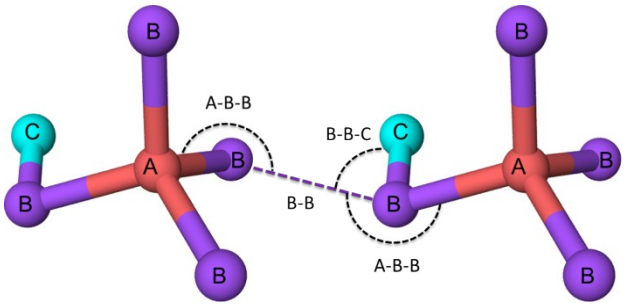

Figure S18. Connection model between two iTBPM molecules.

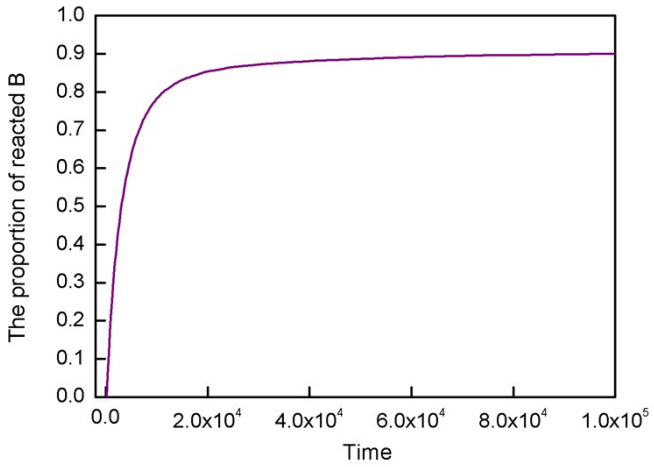

Figure S19. The statistics of the final reacted B particles at the end of the simulation.

S5.2 The algorithm called move-and-grow algorithm is shown and explained below. Testing particles are randomly placed in box with a small diameter (0.2 nm). The testing particles interact with surrounding particles with a potential form.

$$V(r) = \alpha r^2 \left(\frac{1}{r} - \frac{1}{d} \right)^n \qquad r < d \qquad \textit{(eq. 7)}$$

Where α and n are both interaction parameters and d is the diameter of testing particle.

The testing particles move under the forces of surrounding particles.

$$d\vec{s} = dt \cdot \sum \vec{F}_j \qquad \textit{(eq. 8)}$$

And at same time, the diameter of testing particles grows with $d = d + \gamma dt$. The growth of diameter stops when the potential exceeded a threshhold value. For a small growth rate of diameter, the neighboring biggest hole could be detected more often. While for a big growth rate, the local small hole could be over detected. A modest growth rate is suitable for the measurement of the distribution of pore size. We use 10^6 testing particles with n=4, α=200, energy threshhold=10, dt=0.001, and γ=200 for the calculation. When the testing particle stops growth, its diameter could be larger than the size of pore. A visualized pattern of pores and their surroundings according to the move-and-grow algorithm is shown in Fig. S20.

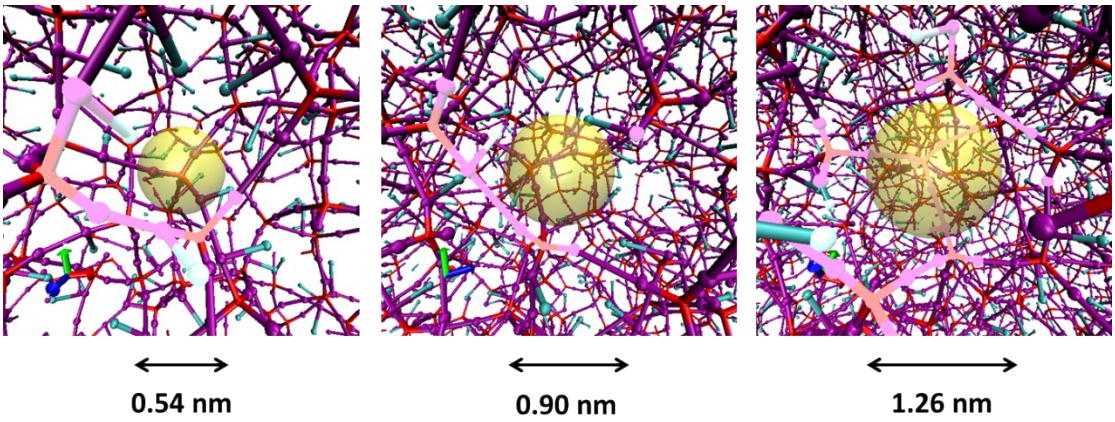

Figure S20. Visualized pattern of pores and their surroundings according to the move-and-grow algorithm.

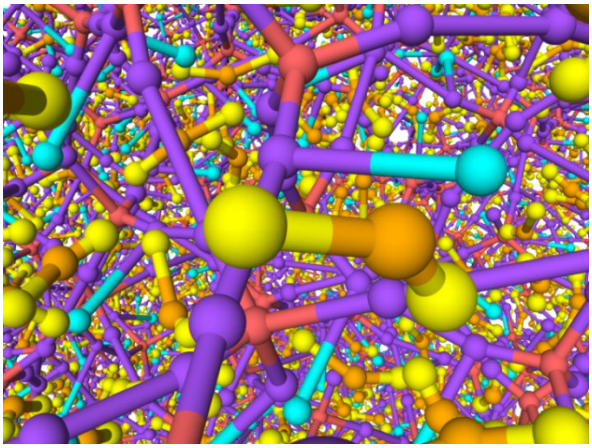

Figure S21. The simulated iPAF-1 with adsorbed DBT molecules under the BE of -36.6 kJ·mol^{-1}.

Section S6. References:

1. S. J. Garibay, M. H. Weston, J. E. Mondloch, Y. J. Colon, O. K. Farha, J. T. Hupp and S. T. Nguyen, *CrystEngComm*, 2013, **15**, 1515-1519.
2. Y. L. Zhu, H. Liu, Z. W. Li, H. J. Qian, G. Milano and Z. Y. Lu, *J. Comput. Chem.*, 2013, **34**, 2197-2211.
3. Y. L. Zhu, D. Pan, Z. W. Li, H. Liu, H. J. Qian, Y. Zhao, Z. Y. Lu and Z. Y. Sun, *Mol. Phys.*, 2018, DOI: 10.1080/00268976.2018.1434904, 1-13.
4. H. Liu, Y. L. Zhu, Z. Y. Lu and F. Müller-Plathe, *J. Comput. Chem.*, 2016, **37**, 2634-2646.